FEM-Based Exterior Workspace Boundary Estimation for Soft Robots via Optimization

Walid Amehri, Gang Zheng, Alexandre Kruszewski

FEM-based Exterior Workspace Boundary Estimation for Soft Robots via Optimization

Walid Amehri, Gang Zheng, and Alexandre Kruszewski

***Abstract*—This paper investigates the exterior workspace boundary of a soft robot with a certain configuration controlled by equipped bounded actuators. To achieve this, we implement an optimization-based approach on the studied soft robot which has been modeled by the Finite Element Method (FEM). Finally, we provide numerical simulations of various configurations to demonstrate the validity of the suggested technique, which, in comparison to the conventional forward method, may considerably minimize the complexity of exterior workspace boundary estimation.**

***Index Terms*—Soft robotics; Workspace boundary; Constrained optimization.**

NOMENCLATURE

n_e	Total number of mesh elements.
n_p	Total number of degrees of freedom.
n_u	Dimension of actuators.
$u \in \mathbb{R}^{n_u}$	Vector of actuation.
$q \in \mathbb{R}^{3n_p}$	Vector of displacements of nodes.
$K(q) \in \mathbb{R}^{3n_p \times 3n_p}$	Matrix of generalized stiffness.
$H^T(q) \in \mathbb{R}^{3n_p \times n_u}$	Force matrix of actuators' direction.
$F(q) \in \mathbb{R}^{3n_p}$	External force vector on the soft robot.
$C \in \mathbb{R}^{3 \times 3n_p}$	Matrix of end-effector entries set to 1.
$q_{_E} \in \mathbb{R}^3$	Vector of end-effector displacement.
$p_{_E} \in \mathbb{R}^3$	Vector of end-effector position.
$\mathcal{U}$	Bounds of the actuation.
$\mathcal{W}_{_E} \in \mathbb{R}^3$	Workspace of the soft robot.
$\partial\mathcal{W}_{_E}$	Workspace boundary of the soft robot.

I. INTRODUCTION

Soft robots are made of deformable materials that may be widely found in the nature, such as rubber, origami, silicone, and several deformable materials [1]. With their natural conformity and low stiffness, they are the safest device for human interaction [2] and the ideal tool for dynamical environments operations [3], resulting in their increasing use in many applications.

However, the process of designing soft robots [4] is still governed by trial-and-error or bio-inspired notions. Given a particular soft robot's configuration, evaluating its reachable workspace is still an open subject, and is very essential for other soft robotics' main scientific challenges, such as control [5], trajectory planning [6], and optimization design [7].

Concerning the modeling techniques, different methods have indeed been reported in the literature for soft robots' flexibility characterization. On the one side, the soft robotics extensively uses the modeling technique PCC (Piece-wise Constant Curvature) [8], but again the constant curvature hypothesis is not always accurate, notably when external stresses are applied on the robot. On the other side, the PCS (Piece-wise Constant Strain) model [9] can be regarded as an extension of the PCC method. This method accounts for both geometric non-linearity and material proprieties, in which a finite group of strain vectors is used to characterize the deformation of the investigated soft robot. The PCS technique, like the PCC method, can only be used to model continuously slender soft robot. In contrast, an appropriate method for modeling the general geometric shape of soft robots is the Finite Element Method (FEM) [10], and may, though at a high dimension model, give a precise soft robots model.

In the literature, various approaches were explored for the workspace estimation of rigid-link mechanisms. In [11], a continuation technique based on bifurcation theory was provided to estimate the workspace boundaries of several rigid-link robots. Next, a method based on analytical study of Jacobian was established in [12] to determine the investigated mechanism unique behavior. Following that, in [13], cables-driven parallel rigid manipulator's wrench-feasible workspace was assessed using interval analysis techniques. Then, an optimization technique to determine the limit of rigid mechanism workspace was suggested in [14]. Despite their excellence in defining the workspace of various types of rigid robots, the strategies noted above cannot be explicitly extended to evaluate the workspace of soft robots since the direct kinematic model explicitly characterizes the input/output (actuation/end-effector position) relation for the rigid case, but such a connection is typically represented in an implicit way by a complex static model for soft robots when modeling the deformation of the soft material, which will be discussed in Section III.

In the soft robotics community, several approaches have been proposed to estimate the workspace of soft robots. A Monte-Carlo based approach was presented in [15] to characterize the workspace of concentric tube continuum robots. In [16], an approximation method was used to determine the workspace boundaries of continuum robots by sweeping the robot from the neutral configuration to the fully curved configuration, for the purpose of deducing the workspace surface from the robot's tip trajectory. The above two workspace estimation approaches are exhaustive since they consist of exploring the inputs domain (actuation domain) which dimension is not stable and may vary corresponding to the investigated soft robot's configuration. Next, an interval analysis based approach using FEM was proposed to estimate the workspace of soft robots [17]. This

Walid Amehri, Gang Zheng and Alexandre Kruszewski are with University of Lille, Inria, CNRS, Centrale Lille, UMR 9189 CRIStAL, F-59000 Lille, France

workspace estimation approach, and even if it consists of discretizing the outputs domain (end-effector domain) which have a stable dimension regardless of the inputs dimension, is still exhaustive in a way that it consists of exploring the whole possible configurations of the workspace instead of mapping its boundary. On the other hand, the work of [18] provides an optimization-based approach that was implemented on the Discrete Cosserat model to estimate the workspace of soft slender manipulators by mapping their exterior workspace boundary. Being inspired by the above work, this paper extends the applicability of the optimization approach by implementing it on the adopted static FEM model [19, p. 428] to estimate the exterior workspace boundary of soft robots. Such an extension is motivated by the following pros. Firstly, FEM can be used to model any type of soft robot, while Cosserat method is limited to model slender type one. Secondly FEM can provide more accurate modeling precision than Cosserat method when modeling soft robots (even for slender type one), since Cosserat theory assumes that all cross-sections (which are perpendicular to the centroidal line of slender soft robots) are rigid and undeformable. Such an assumption is imposed for the sake of modeling simplicity, but inevitably decrease the modeling precision. However, to ensure the above pros (i.e., generality and precision), the price to be paid when using FEM is firstly the resulted high-dimensional model. Therefore there is a trade-off between dimension and precision when fixing the number of elements used to model soft robots. Another price to be paid is the computation complexity: when solving the proposed optimization problem, it is necessary to calculate the gradient of the cost function. Analytical gradient can be deduced when using Cosserat, while it is not possible to have analytical one when using FEM to model soft robots. Consequently, numerical gradient has been used for FEM which increases again the computation time, compared to Cosserat.

II. Problem Statement

We use the structure of a tendon-driven trunk-like soft robot, as illustrated in Fig. 1, to explain clearly the examined topic. Provided the intended soft robot's specific shape, and attached actuators (i.e., tendons) whose amplitudes (i.e., tendons' tension) are in reality limited (noted as $u \in \mathcal{U}$), the point that should be obviously investigated is whether the soft robot's end-effector can achieve the yellow position in Fig. 1 given the existence of a valid input control $u \in \mathcal{U}$?

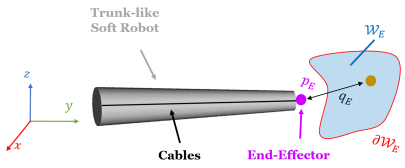

Figure 1: Soft robot and its accessible workspace.

Denote q as the nodal displacement vector, the end-effector position is noted as $p_{_E} \in \mathbb{R}^3$, the end-effector displacement vector with respect to its position $p_{_E}$ is noted as $q_{_E} \in \mathbb{R}^3$. Then the definition of the workspace can be established by:

Definition 1. *Given a soft robot's modeled by $\ddot{q} = \Phi(u, q, \dot{q})$, with a bounded actuator $u \in \mathcal{U}$, the end-effector's $p_{_E} = g(q)$ workspace $\mathcal{W}_{_E}$ is a subspace of $\mathbb{R}^3$, defined below:*

$$\mathcal{W}_{_E} = \{p_{_E} | \exists u \in \mathcal{U}, q, s.t. \Phi(u, q, 0) = 0, p_{_E} = g(q)\}$$

Consistent with Definition 1, the studied problem can be investigated via the ascertainment of the existence of a feasible input $u \in \mathcal{U}$ allowing the containment of the yellow point (depicted in Fig. 1) inside the workspace $\mathcal{W}_{_E}$. Hereafter, the examined topic will be tackled by firstly introducing the studied soft robot's FEM static model, and secondly by implementing two different model-based workspace estimation methods on the designed soft robot.

III. Static Model of Soft Robots

The static model of soft robots is determined using the Finite Element Method in this study. We discretize the flexible field into tiny finite elements n_e to obtain the structure's mesh which contains n_p nodal displacements (equivalently DoFs). Diverse topologies presented in [20] can be used to obtain the mesh of the structure. We adopted the linear tetrahedron element for two primary reasons in this study. On the one hand, using linear tetrahedron elements ensures that the proposed workspace estimation approach can be applied to a variety of soft robot setups and shapes. On the other hand, efficient integration of element matrices can be ensured using linear tetrahedron elements. The selected mesh and the associated discretized representation of the domain are depicted in Fig. 2 for a soft robot in the concept of a trunk.

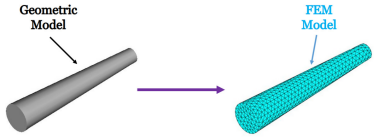

Figure 2: Geometric model and its associated FEM.

The workspace, in agreement with Definition 1, comprises all equilibrium points. We may derive the following static model by applying this property to the robot's motion equation [19, p. 428], which is described by the following equation:

$$K_{_N}(q) = H^T(q)u + F(q) \tag{1}$$

where the nodal displacement vector is represented by $q \in \mathbb{R}^{3n_p}$, the internal force is noted as $K_{_N}(q) \in \mathbb{R}^{3n_p}$, the matrix to describe the actuator direction is noted as $H^T(q) \in \mathbb{R}^{3n_p \times n_u}$, the control input vector is noted as $u \in \mathbb{R}^{n_u}$, the dimension of the inputs is noted as n_u, and the external force vector acting on the soft robot is presented by $F(q) \in \mathbb{R}^{3n_p}$.

Assumption 1. *According to [19, p. 430], the internal forces of the structure $K_{_N}(q)$ can be approximated as:*

$$K_{_N}(q) = K(q)\, q \tag{2}$$

where $K(q)$ can be calculated by putting each element's stiffness matrix together as follows: $K(q) = \sum_{e=1}^{n_e} K_e(q)$, the stiffness matrix of an element e depends on the elasticity matrix ∇, the strain matrix $B_e(q)$, and the volume $V_e(q)$ of the element e. And it can be computed via the following formula [19, p. 429]: $K_e(q) = \int_{V_e(q)} B_e^T(q)\, \nabla B_e(q) dv(q)$.

IV. Exterior Workspace Boundary Estimation

With the workspace being defined in Definition 1 and imposing Assumption 1 on the static model (1), the following is used to govern soft robot's workspace:

$$K(q)\, q = H^T(q)u + F(q) \tag{3a}$$
$$q_{_E} = Cq \tag{3b}$$
$$p_{_E} = q_{_E} + p_{_E}^{(0)} \tag{3c}$$

with the end-effector position being noted as $p_{_E}$, the end-effector's displacement vector with respect to its initial position $p_{_E}^{(0)}$ is denoted by $q_{_E}$, and the matrix of selection related to the node coordinates of the end-effector is symbolized as C.

For all admissible inputs $u \in \mathcal{U}$, estimating $\mathcal{W}_{_E}$ in accordance with (3) can be achieved by calculating the frontiers of $p_{_E}$. However, based on (3), the expression $K(q)q$ varies depending on the material characteristics and is nonlinear, and the input-output mapping $\phi : \mathcal{U} \to \mathcal{W}_{_E}$ is implicit and nonlinear. To this aim, numerical techniques will be applied to estimate the mapping ϕ, and two different manners (the forward method and the optimization-based method) will be studied next.

A. Forward method

Firstly, the mapping ϕ can be iteratively approximated using a classical technique (namely the forward method) which consists of the discretizing the input bound $\mathcal{U}$ and finding the corresponding set of end-effector poses which represents the workspace $\mathcal{W}_{_E}$ of the studied soft robot (as illustrated by Fig. 3).

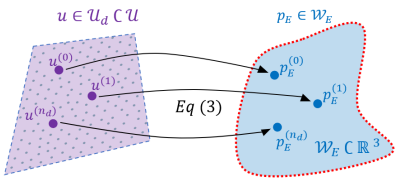

Figure 3: Forward technique.

By discretizing $\mathcal{U}$, we can obtain $\mathcal{U}_d$. Next, given the information of $q^{(j-1)}$ and $p_{_E}^{(j-1)}$ which represent the nodal displacement and the position of the end-effector corresponding at the $(j-1)$th iteration respectively (for $j = 1$, $q^{(0)}$ represents the initial nodal displacement and $p_{_E}^{(0)}$ represents the initial end-effector's position), then for any $u \in \mathcal{U}_d$, we apply Newton-Raphson method to solve (3) and get $q^{(j)}$ by:

$$q^{(j)} = q^{(j-1)} - \Psi_q(u, q^{(j-1)})\, \Psi(u, q^{(j-1)}), \text{ for any } u \in \mathcal{U}_d$$

where $\Psi_q(u, q)$ denotes the gradient of $\Psi(u, q)$ with respect to the nodal displacement vector q, with

$$\Psi(u, q^{(j-1)}) = K(q^{(j-1)})q^{(j-1)} - H^T(q^{(j-1)})u - F(q^{(j-1)})$$

Then, the position of the end-effector with respect to its nodal displacement $q^{(j)}$ is calculated as: $p_{_E}^{(j)} = Cq^{(j)} + p_{_E}^{(0)}$.

Finally, as illustrated in Fig. 3, the estimation of $\mathcal{W}_{_E}$ may be obtained by iterating the aforementioned approach for every possible input $u \in \mathcal{U}_d$.

We would like to emphasize that the computation complexity of this approach is relatively high. In this approach, we have $n_d^{n_u}$ potential possibilities of input u since $u \in \mathcal{U}$ is a subset of $\mathbb{R}^{n_u}$ and the bound for each entry of u is discretized into n_d subsets. In this context, the forward method's computing complexity will increase as the dimension of inputs n_u becomes larger, and will exponentially increase if the discretization precision n_d increases, even if n_u is low.

In the following, a novel technique by discretizing the end-effector domain will be proposed to reduce the computing cost when calculating the workspace of soft robots, rather than discretizing the actuators domain $\mathcal{U}$ with variable dimension.

B. Optimization-based method

The proposed method consists of mapping the surface enveloping soft robots' workspace using numerical algorithms:

1) Firstly, a definition of the workspace boundary, denoted as $\partial\mathcal{W}_{_E}$, is established.
2) Secondly, a ray is emanated from a radiating point v along a certain direction to find a boundary point $p_{_E}^b$ on $\partial\mathcal{W}_{_E}$.
3) In the end, we may get a map of $\partial\mathcal{W}_{_E}$ by finding $p_{_E}^b$ for many consecutive rays with appropriate directions originating at angular intervals.

Finally, as opposed to the forward technique, the suggested optimization-based strategy offers a number of benefits:

1) Since the end-effector space is always less than or equal to 3 (since we are only considering position access), it can reduce the dimension of the space to be discretized;
2) It results in reducing the total number of iterations required to estimate the workspace since it only focuses on finding then mapping the boundary points $p_{_E}^b$ that encloses $\mathcal{W}_{_E}$.

The process for the suggested optimization-based approach is summarized in the steps outlined below:

[Step 1] Establishing the workspace boundary definition $\partial\mathcal{W}_{_E}$;
[Step 2] Determining one point on $\partial\mathcal{W}_{_E}$;
[Step 3] Achieving a map the workspace boundary $\partial\mathcal{W}_{_E}$.

V. Realization of the Optimization-Based Approach

This section will explain the implementation of the proposed optimization-based strategy.

Step 1: Workspace boundary $\partial\mathcal{W}_{_E}$ definition

In accordance with Definition 1, for a specified positive radius ε, the neighborhood of $p_{_E}$ can be defined as: $B_\varepsilon(p_{_E}) = \{\tilde{p}_{_E} \in \mathbb{R}^3 \mid \|p_{_E} - \tilde{p}_{_E}\| < \varepsilon\}$. Using the above statement, we can consistently define the workspace boundary $\partial\mathcal{W}_{_E}$ as:

Definition 2. *The workspace boundary $\partial\mathcal{W}_{_E}$ represents a subset of its workspace $\mathcal{W}_{_E}$, and can be defined as follows:*

$$\partial\mathcal{W}_{_E} = \{p_{_E} \in \mathcal{W}_{_E} \mid \forall\varepsilon > 0, \exists\tilde{p}_{_E} \in B_\varepsilon(p_{_E}), s.t.\ \tilde{p}_{_E} \notin \mathcal{W}_{_E}\}$$

Step 2: A single point on $\partial\mathcal{W}_E$ determination

In this step, we explain how to find an initial boundary point p_E^b on the workspace boundary $\partial\mathcal{W}_E$ (as depicted via a simplified illustration in Fig. 4). In fact, this step is necessary and needs to be treated before we proceed toward mapping the workspace enclosing surface.

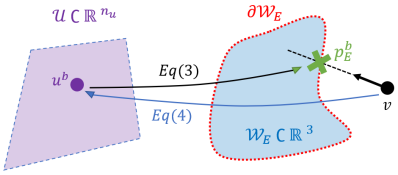

Figure 4: Calculate related actuation u^b for a radiating v using (4), then derive associated boundary point p_E^b using (3).

A boundary point p_E^b in a specific direction emerging from a radiating point v that is external to the workspace $\mathcal{W}_E$ (as represented by Fig. 4) may be found in accordance with Definition 2 by solving the constrained optimization problem defined below:

$$\begin{aligned} [u^b, q^b] = \arg\min_{u,q} \quad & \|p_E(q) - v\|_2^2 \\ \text{s.t.} \quad & u \in \mathcal{U} \text{ and (3)} \end{aligned} \tag{4}$$

where the obtained actuation u^b and its associated displacement vector q^b represent the optimal and feasible solution (since they satisfy the bounded constraint and the nonlinear constraints) to minimize the distance between $p_E(q)$ and v. Finally, we deduce the related end-effector boundary position using the following: $p_E^b = Cq^b + p_E^{(0)}$.

The radiating point v should be outside the workspace, as indicated in Fig. 4. For this, we simply have to select v such that $||\vec{Ov}|| > L_{\max}$, where $O = [0,0,0]^T$ is the origin of the reference frame, since in practice the length L of a soft robot is bounded by $L_{\max}$.

Step 3: Workspace boundary $\partial\mathcal{W}_E$ mapping

The final step consists of mapping the workspace boundary $\partial\mathcal{W}_E$ by employing a numerical technique. To realize this, we can proceed by finding the boundary points corresponding to multiple successive directions (as described by a simplified illustration in Fig. 5).

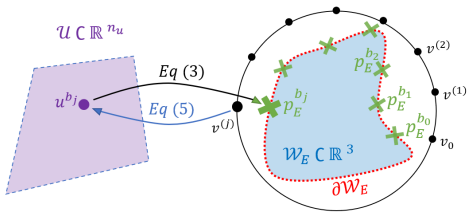

Figure 5: Calculate related actuation u^{b_j} for a radiating $v^{(j)}$ using (5), then derive associated boundary point $p_E^{b_j}$ using (3).

Precisely, with v_0 being the initial radiating vector that can be calculated based on the technique proposed in Step 2, and the rotation matrix $R_\delta^{(j)}$ is established by: $R_\delta^{(j)} = R_{\delta_x^{(j)}} R_{\delta_y^{(j)}} R_{\delta_z^{(j)}}$, with $R_{\delta_x^{(j)}}$, $R_{\delta_y^{(j)}}$, and $R_{\delta_z^{(j)}}$ denoting the basic matrices of rotation with respect to the x, y and z axis respectively. Thus, the direction vector $v^{(j)}$ is equal: $v^{(j)} = R_\delta^{(j)} v_0$. Then, given n_d successive rays, with respective directions $v^{(j)}$, $j = 0, \ldots, n_d$ emanating from an initial radiating point v_0 at angular intervals of δ_x, δ_y and δ_z (with $\delta_{x,y,z} = 2\pi/n_d$), the workspace boundary can be numerically mapped by solving the following optimization problem:

$$\begin{aligned} [u^{b_j}, q^{b_j}] = \arg\min_{u,q} \quad & \|p_E(q) - v^{(j)}\|_2^2 \\ \text{s.t.} \quad & u \in \mathcal{U} \text{ and (3)} \end{aligned} \tag{5}$$

where the achieved actuation vector u^{b_j} and its associated displacement vector q^{b_j} are the optimal and feasible solution to minimize the distance between $v^{(j)}$ and p_E. Accordingly, the associated end-effector boundary position can be deduced as: $p_E^{b_j} = Cq^{b_j} + p_E^{(0)}$.

Non-convexity issues and proposed solution

The process of mapping the workspace boundary $\partial\mathcal{W}_E$ may sometimes be confronted with non-convexity difficulties which might lead to an overestimation of the workspace, as depicted by the following illustration (refer to Fig. 6). When this situation occurs ($\|p_E^{b_{n_1}} - p_E^{b_{n_2}}\|_2 > r$), it is possible that either $p_E^{b_{n_1}}$ or $p_E^{b_{n_2}}$ will be the only achievable solutions of (5) for all direction vectors $v^{(j)}$ between $v^{(n_1)}$ and $v^{(n_2)}$, i.e.,

$$\forall v^{(j)} \in [v^{(n_1)}\ v^{(n_2)}],\ (5) \implies p_E^{b_{n_1}} \text{ or } p_E^{b_{n_2}}$$

As a result, we may miss the identification of the turquoise colored boundary points in Fig. 6

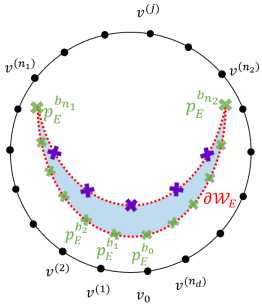

Figure 6: Non-convexity $\partial\mathcal{W}_E$: sudden jump from $p_E^{b_{n_1}}$ to $p_E^{b_{n_2}}$.

The phenomenon yielding such a problem can be tracked down by recognizing an abrupt jump resulted from (5) between two successive iterations of at least one actuation $u_k^{b_j} \in u^{b_j}$. Accordingly, once such a situation is detected, this paper proposes a strategy that will allow us to completely identify the probably missed turquoise colored boundary points in Fig. 6. This technique focuses firstly on obtaining a list of radiating points v_l by discretizing the space between $p_E^{b_{n_1}}$ and $p_E^{b_{n_2}}$ as shown in Fig. 7. Afterwards, we solve (4) for each point the obtained list v_l, and get their related boundary points. Finally, we can successfully identify the boundary points lying on the non-convex part, and achieve the correct estimation of the workspace boundary (as illustrated in Fig. 7).

The proposed strategy can be summarized as follows:

[Step. A] Calculate the set of v_l by discretizing the space between $p_E^{b_{n_1}}$ and $p_E^{b_{n_2}}$;

[Step. B] Compute the related feasible solution by solving (4) for each discretized point v_l, then deduce its corresponding boundary point.

To clearly understand the above steps, we present a successive iteration in Fig. 7 to illustrate the proposed strategy.

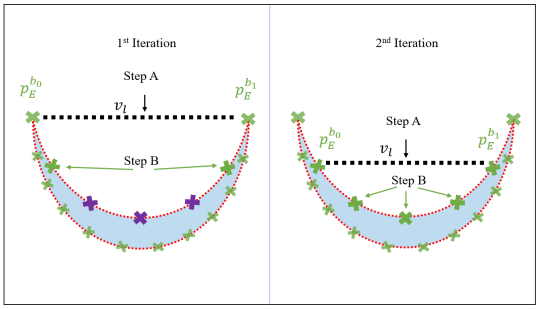

Figure 7: Non-convexity solution: for v_l, calculate its related actuation via (4) and deduce its associated boundary via (3).

Realization of the algorithm

The suggested optimization-based approach with the selected strategy to resolve the non-convexity issue is described in a concise algorithm (See Algorithm 1).

Algorithm 1 Calculate $\partial\mathcal{W}_E$

Require: $v_0, C, \mathcal{U}, n_d, n_s, r, p_E^{(0)}$
  $\delta \leftarrow 2\pi/n_d$; $\partial\mathcal{W}_E \leftarrow \varnothing$; ▷ Initialization
  for $j \leftarrow 1$ to n_d **do**
    $v^{(j)} \leftarrow R_\delta^{(j)}\ v_0$ ▷ Direction vector
    $[u^{b_j}, q^{b_j}] \leftarrow solve_{(5)}(v^{(j)}, C, \mathcal{U}, p_E^{(0)})$ ▷ Optimal solution
    $p_E^{b_j} \leftarrow Cq^{b_j} + p_E^{(0)}$ ▷ Boundary point
    $\partial\mathcal{W}_E \leftarrow \partial\mathcal{W}_E \oplus p_E^{b_j}$ ▷ Append
    if $\|p_E^{b_{j-1}} - p_E^{b_j}\|_2 > r$ **then** ▷ Non-convexity
      $v_l \leftarrow dis(p_E^{b_{j-1}}, p_E^{b_j}, n_s)$ ▷ Discretize
      for $s \leftarrow 1$ to n_s **do**
        $[u^{b_s}, q^{b_s}] \leftarrow solve_{(4)}(v_l^{(s)}, C, \mathcal{U}, p_E^{(0)})$
        $p_E^{b_s} \leftarrow Cq^{b_s} + p_E^{(0)}$ ▷ Boundary point
        $\partial\mathcal{W}_E \leftarrow \partial\mathcal{W}_E \oplus p_E^{b_s}$ ▷ Append
      end for
    end if
  end for

VI. Validation and Analysis

In this section, we illustrate the presented results by evaluating the reachable workspace of a trunk-like soft robot with a Young's modulus $E = 1.8 \times 10^7 Pa$, and a Poisson ratio $\nu = 0.45$. The following presented scenarios were conducted on an Intel Xeon(R) processor with 16 GB of RAM and a 3.50 GHz clock speed. We investigate three situations in which a trunk-like soft robot is actuated by various tendon routing configurations, and we use simultaneously the forward and optimization-based approaches to estimate the accessible workspace $\mathcal{W}_E$ and the exterior workspace boundary $\partial\mathcal{W}_E$ for every case. For each situation, the outcomes of both techniques are superimposed and shown by a three-view graphic (Oxy, Ozy, and Ozx plans). We suggest discretizing the actuation vector with a step size of 1 Newton (unit) for the forward method, and discretizing the angles with a discretization step size of 0.08 Radian for the optimization-based approach.

A. Scenario 1: 2 tendons-driven trunk-like soft robot

The first scenario is the trunk-like soft robot operated by two tendons (as illustrated in Fig. 8a). We exert a force with a magnitude within $\mathcal{U}^{(0)} = \mathcal{U} = [0\ 100] \times [0\ 100]$.

Using the explanation outlined in Section IV-A, we first use the forward approach with $n_d = 100$ to obtain the related estimation of $\mathcal{W}_E$ for this soft robot's configuration (represented by blue colored points in 8b, 8c and 8d). The forward technique needs $n_d^{n_u} = 100^2$ operations in terms of operation complexity, and it takes about 1463 seconds to compute the complete estimation of this scenario workspace in terms of time computation.

For the same scenario, the optimization-based approach required a total number of 864 operations with a time computation of 984 seconds. The obtained boundary points are depicted by green colored points in Figs. 8b, 8c and 8d, which represent the exterior workspace boundary $\partial\mathcal{W}_E$ of this soft robot's configuration.

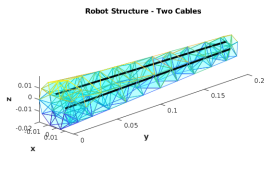

(a) Soft Robot with $n_u = 2$.

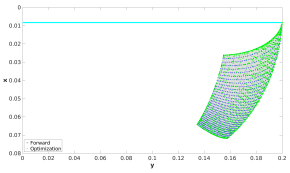

(b) Oxy plan view.

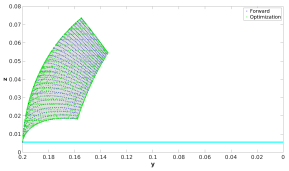

(c) Ozy plan view.

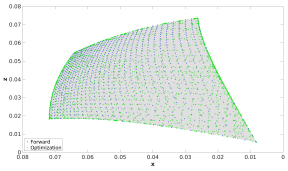

(d) Ozx plan view.

Figure 8: Scenario 1: Forward method to get $\mathcal{W}_E$ (blue points) and optimization-based method to get $\partial\mathcal{W}_E$(green points)

.

B. Scenario 2: 3 tendons-driven trunk-like soft robot

The second scenario considers the trunk-like soft robot operated by three tendons (as illustrated in Fig. 9a). We apply a force magnitude within $\mathcal{U}^{(0)} = \mathcal{U} = [0\ 100] \times [0\ 100] \times [0\ 100]$.

The forward approach is firstly applied with $n_d = 100$ to obtain this configuration's workspace $\mathcal{W}_E$ (illustrated in Figs. 9b, 9c, and 9d by blue-colored points). The forward technique needs $n_d^{n_u} = 100^3$ operations, and 1.4×10^5 seconds to achieve the entire estimation of this scenario's workspace. Next, using Step. 3 (Fig. 5) of the optimization-based approach with $n_{d_z} = 72$ and $n_{d_x} = 12$, we map the boundary points of this particular configuration. For this scenario, the proposed

optimization-based approach required a total number of 864 operations with a time computation of 1034 seconds. The achieved boundary points are illustrated by green colored points in Figs. 9b, 9c, and 9d, which represent the workspace boundary $\partial\mathcal{W}_E$ of this particular configuration.

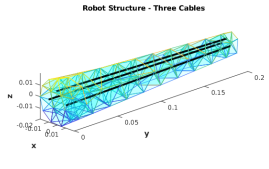

(a) Soft Robot with $n_u = 3$.

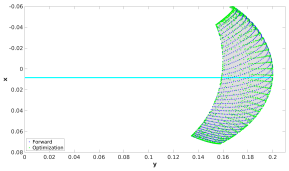

(b) Oxy plan view.

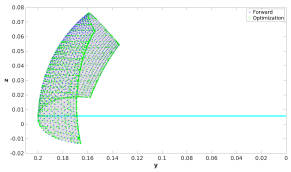

(c) Ozy plan view.

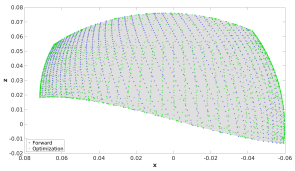

(d) Ozx plan view.

Figure 9: Scenario 2: Forward method to get $\mathcal{W}_E$ (blue points) and optimization-based method to get $\partial\mathcal{W}_E$(green points)

.

C. *Scenario 3:* 4 *tendons-driven trunk-like soft robot*

The third scenario considers the trunk-like soft robot operated by four symmetric tendons (as illustrated in Fig. 10a). We apply a force whose magnitude within a specific range $\mathcal{U}^{(0)} = \mathcal{U} = [0\ 100]_1 \times \cdots \times [0\ 100]_4$.

The forward approach is firstly applied with $n_d = 100$ to obtain this configuration's workspace $\mathcal{W}_E$ (illustrated by blue colored points in Figs. 10b, 10c and 10d). The forward technique needs $n_d^{n_u} = 100^4$ operations, and 1.4×10^7 seconds to completely estimate this scenario's workspace. Then, we use Step. 3 (Fig. 5) of the optimization-based approach with $n_{d_z} = 72$ and $n_{d_x} = 12$ to map the boundary points of this particular configuration. For this scenario, the optimization-based approach required a total number of 864 operations with a time computation of 1039 seconds. The obtained boundary points are depicted by green colored points in Figs. 10b, 10c and 10d, which represent the workspace boundary $\partial\mathcal{W}_E$ of the studied soft robot's configuration.

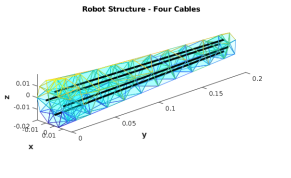

(a) Soft Robot with $n_u = 4$.

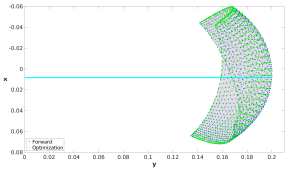

(b) Oxy plan view.

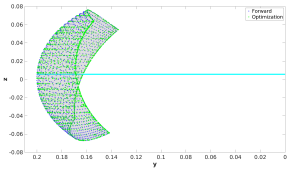

(c) Ozy plan view.

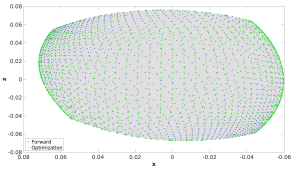

(d) Ozx plan view.

Figure 10: Scenario 3: Forward method to get $\mathcal{W}_E$ (blue points) and optimization-based method to get $\partial\mathcal{W}_E$(green points)

.

D. *Notes on scenario results*

Based on the achieved results, we can clearly see from the three-view drawing of each scenario that the workspace boundary estimation result achieved via the optimization-based method encloses the estimated workspace obtained via the forward approach. Furthermore, when matched to the forward technique, the suggested optimization-based methodology may achieve equivalent workspace estimation accuracy while decreasing the number of operations and the amount of time it takes to estimate the workspace for each scenario.

E. *Notes on computation complexity*

We summarize the operations complexity and time calculation for every scenario in the following tables (see Tables I and II), where the time computation of the forward method for configurations with $n_u \geqslant 3$ is merely estimated since they need a very lengthy time.

Table I: Comparison of operations complexity.

Approach / Inputs	Operations	
	Forward	Optimization
$n_u = 2$	10^4	864
$n_u = 3$	10^6	864
$n_u = 4$	10^8	864

Table II: Comparison of computational time.

Approach / Inputs	Time (seconds)	
	Forward	Optimization
$n_u = 2$	1463	984
$n_u = 3$	$\approx 1.4 \times 10^5$	1034
$n_u = 4$	$\approx 1.4 \times 10^7$	1039

In addition, we can also illustrate the complexity of operations and the time computation by Figs. 11a and Fig. 11b, where it can be seen how expanding the dimension of the

actuators has an exponential effect on the forward method, but the suggested optimization-based approach's is essentially linearly stable.

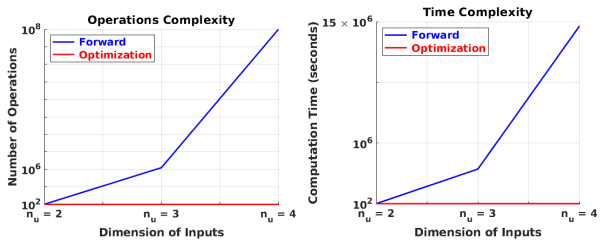

(a) Operations complexity. (b) Time Computation

Figure 11: Comparison of operations complexity and time computation for forward method and optimization method.

F. Notes on limitation

This paper proposed an optimization-based approach to efficiently estimate the workspace boundary of soft robots. The proposed optimization-based approach consists of mapping the surfaces enclosing the workspace, i.e., this approach can only successfully identify the points that constitutes the exterior boundary of the workspace. Although this approach has such a limitation, however as shown in [18], the optimization-based approach can effectively and successfully map the exterior boundaries of multisection soft robots actuated by a generic dimension of tendons.

VII. Conclusions

This paper proposed two different workspace estimation approaches for soft robots modeled by the FEM method. On one side, we provided a classic strategy, namely the forward approach, which discretizes the actuators' space in order to estimate the workspace of a soft robot. In contrast, we have suggested a specific optimization-based technique for reducing the forward method's computing cost, by mapping the exterior workspace boundary of soft robots and avoiding the costly calculation of inside configurations. Ultimately, utilizing the forward technique as a comparison reference, a validation of the suggested strategy was achieved using several configurations of soft robots. In comparison to the simple forward approach, which exponentially expands as the actuator's size rises, we have demonstrated the optimization-based approach efficiency.

References

[1] F. Iida and C. Laschi, "Soft robotics: challenges and perspectives," *Procedia Computer Science*, vol. 7, pp. 99–102, 2011.

[2] S. Yim and M. Sitti, "Design and rolling locomotion of a magnetically actuated soft capsule endoscope," *IEEE Transactions on Robotics*, vol. 28, no. 1, pp. 183–194, 2012.

[3] R. F. Shepherd, F. Ilievski, W. Choi, S. A. Morin, A. A. Stokes, A. D. Mazzeo, X. Chen, M. Wang, and G. M. Whitesides, "Multigait soft robot," *Proceedings of the national academy of sciences*, vol. 108, no. 51, pp. 20 400–20 403, 2011.

[4] D. Rus and M. T. Tolley, "Design, fabrication and control of soft robots," *Nature*, vol. 521, no. 7553, pp. 467–475, 2015.

[5] C. Della Santina, R. K. Katzschmann, A. Biechi, and D. Rus, "Dynamic control of soft robots interacting with the environment," in *2018 IEEE International Conference on Soft Robotics (RoboSoft)*. IEEE, 2018, pp. 46–53.

[6] K. Wu and G. Zheng, "Fem-based gain-scheduling control of a soft trunk robot," *IEEE Robotics and Automation Letters*, vol. 6, no. 2, pp. 3081–3088, 2021.

[7] J. Hiller and H. Lipson, "Automatic design and manufacture of soft robots," *IEEE Transactions on Robotics*, vol. 28, no. 2, pp. 457–466, 2011.

[8] R. J. Webster III and B. A. Jones, "Design and kinematic modeling of constant curvature continuum robots: A review," *The International Journal of Robotics Research*, vol. 29, no. 13, pp. 1661–1683, 2010.

[9] F. Renda, F. Boyer, J. Dias, and L. Seneviratne, "Discrete cosserat approach for multisection soft manipulator dynamics," *IEEE Transactions on Robotics*, vol. 34, no. 6, pp. 1518–1533, 2018.

[10] G. Zheng, O. Goury, M. Thieffry, A. Kruszewski, and C. Duriez, "Controllability pre-verification of silicone soft robots based on finite-element method," in *2019 International Conference on Robotics and Automation (ICRA)*. IEEE, 2019, pp. 7395–7400.

[11] E. J. Haug, C.-M. Luh, F. A. Adkins, and J.-Y. Wang, "Numerical algorithms for mapping boundaries of manipulator workspaces," *Journal of Mechanical Design*, vol. 118, no. 2, pp. 228–234, 1996.

[12] K. Abdel-Malek and H.-J. Yeh, "Analytical boundary of the workspace for general3-dof mechanisms," *The International Journal of Robotics Research*, vol. 16, no. 2, pp. 198–213, 1997.

[13] M. Gouttefarde, D. Daney, and J.-P. Merlet, "Interval-analysis-based determination of the wrench-feasible workspace of parallel cable-driven robots," *IEEE Transactions on Robotics*, vol. 27, no. 1, pp. 1–13, 2010.

[14] J. Snyman, L. Du Plessis, and J. Duffy, "An optimization approach to the determination of the boundaries of manipulator workspaces," *Journal of Mechanical Design*, vol. 122, no. 4, pp. 447–456, 2000.

[15] J. Burgner-Kahrs, H. B. Gilbert, J. Granna, P. J. Swaney, and R. J. Webster, "Workspace characterization for concentric tube continuum robots," in *2014 IEEE/RSJ International Conference on Intelligent Robots and Systems*. IEEE, 2014, pp. 1269–1275.

[16] K. Cao, R. Kang, D. T. Branson III, S. Geng, Z. Song, and J. S. Dai, "Workspace analysis of tendon-driven continuum robots based on mechanical interference identification," *Journal of Mechanical Design*, vol. 139, no. 6, p. 062303, 2017.

[17] W. Amehri, G. Zheng, and A. Kruszewski, "Fem based workspace estimation for soft robots: a forward-backward interval analysis approach," in *2020 3rd IEEE International Conference on Soft Robotics (RoboSoft)*. IEEE, 2020, pp. 170–175.

[18] W. Amehri, G. Zheng, A. Kruszewski, and F. Renda, "Discrete cosserat method for soft manipulators workspace estimation: an optimization-based approach," *Journal of Mechanisms and Robotics, in press*, 2021.

[19] S. S. Rao, *The finite element method in engineering*. Butterworth-heinemann, 2017.

[20] J. Reddy, *An introduction to the finite element method*. McGraw-Hill New York, USA, 2013, vol. 1221.